Sensors and Actuators B 259 (2018) 475–483

Contents lists available at ScienceDirect

Sensors and Actuators B: Chemical

journal homepage: www.elsevier.com/locate/snb

Electrothermal silver nanowire thin films for In-Situ observation of thermally-driven chemical processes

Eduardo D. Martínez[a,*], Alí F. García Flores[b], Hernán Pastoriza[c], Ricardo R. Urbano[a], Carlos Rettori[a,b]

[a] "Gleb Wataghin" Institute of Physics (IFGW), University of Campinas (UNICAMP), 13083-859, Campinas, SP, Brazil
[b] CCNH, Federal University of ABC (UFABC), 09210-580, Santo André, SP, Brazil
[c] División Bajas Temperaturas, Centro Atómico Bariloche, Comisión Nacional de Energía Atómica, CONICET, Av Bustillo 9500, S.C. Bariloche, R8402AGP, Río Negro, Argentina

ARTICLE INFO

Article history:
Received 4 October 2017
Received in revised form
22 November 2017
Accepted 4 December 2017
Available online 13 December 2017

Keywords:
Silver nanowires
Nanocomposites
Electrothermal device
Transparent conductors
Gold nanoparticles
pNIPAM

ABSTRACT

We develop a novel device comprised of high optical transmittance thin films containing silver nanowires (AgNWs) in poly(methyl methacrylate) (PMMA) acting as heating elements. The electrothermal control of the AgNWs network allows us to externally trigger and tune the temperature conditions required to run chemical reactions and physicochemical processes. The device was successfully applied for the spectroscopic in-situ observation of three different model reactions: i) the thermal equilibrium of a $CoCl_2/HCl/H_2O$ complex, ii) the reversible macromolecular phase transition of a pNIPAM solution, and iii) the nucleation and growth of gold nanoparticles (AuNPs). In the first case, the color of the Co^{2+} complex was reversibly switched from pink to blue when changing the thermal equilibrium condition. In the second one, the optical transmittance of an aqueous solution of carboxylic-terminated pNIPAM polymer was cycled from high to low as the temperature of the solution was below or above the lower critical solubility temperature (LCST) respectively. Finally, the electrothermal control on the device was applied to the study of the nucleation and growth of AuNPs in an organic solution of $AuCl_3$ containing oleylamine acting as both the reducer and the stabilizing agent. The versatility of the electrothermal device provides an easy way to undertake thermally controlled processes and develop optical elements such as smart windows and lab-on-a-chip devices. The AgNWs-PMMA nanocomposite was also applied successfully as an electrothermal ink on the external side walls of a test tube.

1. Introduction

Development of polymer-based nanocomposite materials aims to combine in a synergistic way the properties of nanoscale additives with those of bulk polymer matrices. While additives are incorporated to enhance the mechanical, electrical, magnetic or optical properties of the composite materials, polymers play the important role of providing convenient processing properties, corrosion-protective environments for the additives and mechanical flexibility of the final products. One of such examples of nanocomposites is that of polymers containing silver nanowires (AgNWs). AgNWs form percolating networks with high electrical conductivity and low metal content [1–4] producing highly transparent electrodes in the form of thin films. In this regard, AgNWs networks stand as the most studied candidate to replace indium tin oxide (ITO) as a transparent conductor, especially for flexible electronics [5–7]. Different formulations for AgNWs inks and coating procedures to obtain high transparency, low haze, and low sheet resistance have been proposed in the last few years, including patterning techniques [8,9]. Furthermore, the well-known Joule effect by which the current flow through the AgNWs network dissipates energy in the form of heat has also been previously exploited in order to form transparent heating coatings [10,11]. Applications such as defrosting windows have been proposed in the past [12,13]. In addition, patterning techniques were recently developed to produce micrometer sized features on both rigid and flexible substrates using the AgNWs-poly(methy methacrylate) (PMMA) nanocomposite, either by electron beam lithography or by soft lithography techniques [9]. On the other hand, the local heating of individual AgNWs have shown to result in a much faster and more efficient electro-thermochemical reaction than bulk heating [14], allowing,

* Corresponding author.
E-mail addresses: edmartin@ifi.unicamp.br, edmartin@cnea.gov.ar (E.D. Martínez).

https://doi.org/10.1016/j.snb.2017.12.021
0925-4005/

for example, the localized thermochemical growth of ZnO [15]. Besides their use as heater elements, AgNWs have been applied, using diverse processing techniques, in a plethora of technologies summarized in recent reviews [16–18].

In this work, we extend those advances even further by developing a simple device where a thin film composed of AgNWs dispersed in PMMA was used as a transparent heating element allowing the external electrothermal control of the local temperature. By using this device, several physicochemical phenomena could be analyzed in-situ by means of UV–vis transmission spectrophotometry. Specifically, three chemical processes with a clear optical feature but completely different in nature were studied using this methodology.

The first case is the well-known optical absorption changes that take place when the equilibrium of the cobalt(II) chloride complex in aqueous solution is thermally disrupted. In the second case, we analyzed the thermoresponsive polymer pNIPAM. This material undergoes a solubility phase transition at a critical temperature known as the lower critical solution temperature (LCST), close to 32 °C for pure aqueous solutions [19,20]. Finally, a more complex chemical reaction was investigated using our developed device. The synthesis of gold nanoparticles (AuNPs) can be achieved by a plethora of methods, many of them performed at a constant temperature with a rapid injection of a chemical reducer, as is the case of the classical Turkevich method [21], or by phase transfer techniques, as that from Brust et al.[22]. In any of these cases, the nucleation and growth of AuNPs is so fast that it is difficult to follow in real time the evolution of the localized surface plasmon resonance (LSPR). However, other synthesis procedures were already developed where the kinetics of particle formation is slower and can be controlled by adjusting the relevant parameters. One of these methods is the reduction of $AuCl_4^-$ by oleylamine (OLA) [23]. In this reaction, OLA acts also as a stabilizing agent by forming a capping layer on the formed AuNPs. As reported by Liu et al. [24], the AuNPs-OLA synthesis can be followed by UV–vis spectrophotometry provided that the necessary equipment for the thermal control is available, which is not often the case. In this work, we modified the mentioned synthesis procedure in order to test the applicability of our device for the in-situ study of AuNPs growth.

We call the attention on the different nature of the chemical processes presented in this study; chemical equilibrium, solubility phase transition and nanoparticle synthesis, all of them analyzed using the same device. All these cases represent just examples of the viabilities of the proposed device, where their fabrication provides an accessible tool to perform thermally controlled experiments, not only restricted to optical studies. We provide here the unique features of a nanocomposite material based on AgNWs and PMMA to develop a simple, yet robust and versatile, useful device.

2. Experimental

2.1. Synthesis of silver nanowires

The construction of the device starts with the synthesis of AgNWs by the polyol method [25]. In this procedure, $AgNO_3$ is the metal precursor, polyvinylpyrrolidone (PVP) is the structuring agent which preferentially binds on the (100) faces of the nucleated silver nanocrystals promoting the anisotropic growth of the nanowires in the [110] direction. Ethylenglycol (EtGOH) acts both as the solvent and the reducer. In a batch synthesis, more than 100 mg of AgNWs can be extracted [26]. Importantly, this procedure was reported to be scalable up to one gram of AgNWs per batch [27]. More details about the synthesis are provided in the Methods section. The AgNWs after extraction were dispersed in isopropanol (IPA) in a weight concentration of 2.5 g L^{-1}. For the preparation of the nanocomposite, 2 ml of the AgNWs colloid in IPA were centrifuged at 1000 rpm (174 relative centrifugal force) and the supernatant was discarded. Then, 200 ml of a PMMA solution, 7% wt. in chlorobenzene, was added followed by vortex agitation to homogenize the mixture. The as-obtained AgNWs-ink could be used to form a thin film via spin coating or be applied as a conductive ink which cures at room temperature.

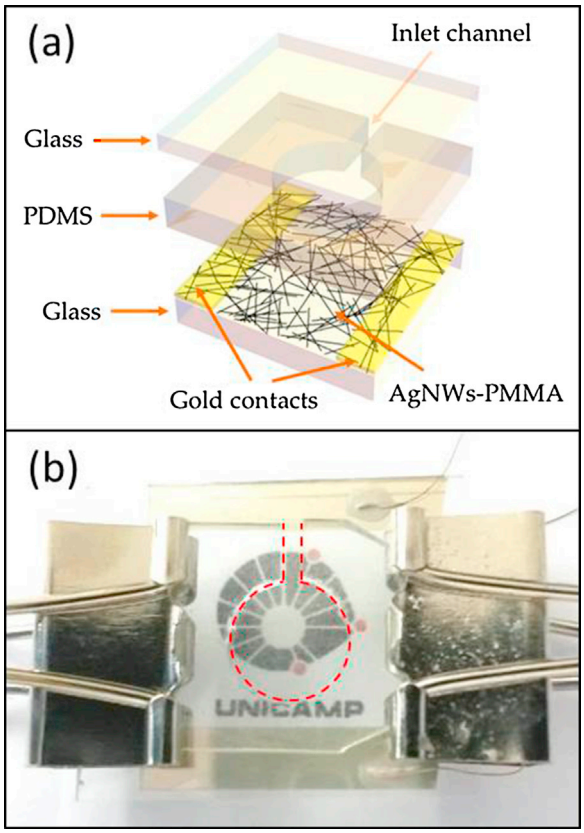

Fig. 1. Scheme (a) and picture (b) of the electrothermal device comprising a nanocomposite film of AgNWs in PMMA, a PDMS spacer with a reservoir and an inlet channel (marked in red dashed line) and a cover glass slide. (For interpretation of the references to colour in this figure legend, the reader is referred to the web version of this article.)

2.2. Preparation of the device

For building the device, a film was deposited by spin coating at 3000 rpm for 60 s on glass substrates and then heated at 180 °C for 2 min in a hot plate. As an option, but not mandatory, gold contacts were sputtered on the extremes of the substrate prior to the film deposition to facilitate the wire bonding using silver paste and thin copper wires. The AgNWs nanocomposite film on the glass substrate constitutes the heating element of the device. A second component acting as the spacer and reservoir of the solutions to be studied was made with poly(dimethylsiloxane) (PDMS). A sheet of this material was prepared (Methods section) and cut to the appropriate size. The reservoir region was also cut with a circular hollow punch and an inlet channel was cut manually. Finally, a glass slide was placed on top and office clamps were used to compress the PDMS sheet and seal the device. The final thickness of the PDMS spacer was (1.7 ± 0.1) mm. A scheme and a picture of the device are shown in Fig. 1. The calibration of the device (electrical power vs. temperature) was performed by placing a calibrated thermocouple in the reservoir filled with water. To perform the in-situ experiments, the device without any content in the reservoir was used as blank for the absorbance/transmittance measurements

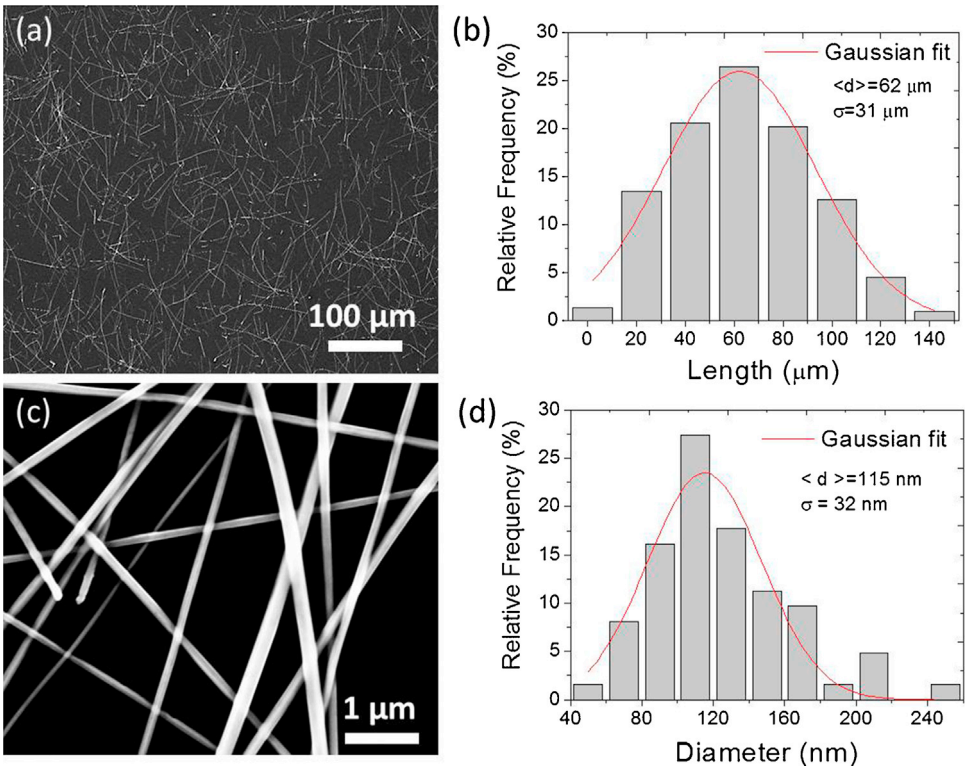

Fig. 2. Characterization of AgNWs by SEM analyses. SEM images (a, c) and statistical counting analysis of nanowires length (b) and diameter (d).

in a UV–vis spectrophotometer. The prepared solutions (Methods section) were then placed in the reservoir by using a syringe. A DC power supply was set to the appropriate output voltage and switched ON and OFF either manually or by using a relay controlled by an Arduino board. The acquisition was set automatically in the spectrophotometer to register the absorption spectra at regular time intervals.

3. Results and discussion

Silver nanowires were characterized by optical and scanning electron microscopy (SEM) after the synthesis as shown in Fig. 2. Although there is a broad dispersion in size, characteristic values of (60 ± 30) µm in length and (115 ± 30) nm in diameter were extracted from statistical analysis of several SEM images. On the other hand, the nanocomposite films formed by AgNWs and PMMA after curing were characterized by SEM and atomic force microscopy (AFM) as shown in Fig. 3a,b. The films present a random arrangement of AgNWs with no preferential orientation. AFM shows a rough surface with heights and valleys up to 100 nm, as expected from the diameter of the nanowires. A step was formed by scratching the film in order to measure its thickness (Fig. 3c,d). A thickness of (1.0 ± 0.1) µm was obtained after fitting the step height in the line profile indicated in Fig. 3c. The nanocomposite film displays a sheet resistance of $(2.0 \pm 0.1)\ \Omega\ sq^{-1}$ as determined by 4-probes measurements. The calibration was performed by placing a thermocouple in the reservoir filled with water. Different DC voltages were applied while registering the current flowing through the AgNWs-PMMA nanocomposite film and the temperature value indicated by the thermometer (Fig. 4a). A linear relation was found although a slight deviation was observed for power values above 1.2 W. The temperature range attainable is from room temperature up to 70 °C. The optical transmittance of the film at 550 nm was measured to be 67% (Fig. 4b).

3.1. Thermal equilibrium of a cobalt chloride aqueous complex

The application of the device for the in-situ characterization of thermally dependent absorption spectra was first tested using a cobalt chloride complex. According to Le Châtelierí's principle, the equilibrium constant of the following reaction (Eq. (1)) is temperature-dependent

$$[Co(H_2O)_6]^{2+}(aq., pink) + 4Cl^- \overset{\Delta}{\rightarrow} [CoCl_4]^{2-}(aq., blue) + 6H_2O \quad (1)$$

Furthermore, the characteristic color of each cobalt complex arises from the different crystal field splitting. Therefore, a color change occurs when the reaction is shifted from the left to the right side of Eq. (1), for example, by providing heat (Δ) and increasing the temperature.

A cobalt chloride aqueous solution containing HCl was placed in the reservoir of the device and the automatic absorption acquisition was started with a 30 s period between measurements. The DC voltage source was set to 8 V output but remained OFF for the first two minutes of the experiment. The spectral changes are displayed in Fig. 5a where two main absorption bands in the visible region are clearly distinguishable. The first band, centered at 520 nm is present from the beginning of the experiment, *i.e.* at room temperature (22 °C), and accounts for the pink color of the solution. When the power source is turned ON, a current flow was measured to be (0.21 ± 0.02) A, corresponding to a total electrical power of (1.6 ± 0.1) W, which represents a final temperature of 71 °C. From this moment on, a second absorption band, centered at 664 nm, begins to increase its relative intensity until it becomes the predominant feature of the solution, giving its blue coloration. As explained in the Introduction section, each of these colors correspond to the $[Co(H_2O)_6]^{2+}$ and the $[CoCl_4]^{2-}$ complexes. The experiment shows the change in the chemical equilibrium when temperature is increased and the endothermic nature of the reaction displayed in Eq. (1). The trends of each band during the heating and cooling cycle after the subtraction of the baseline are shown in Fig. 5b.

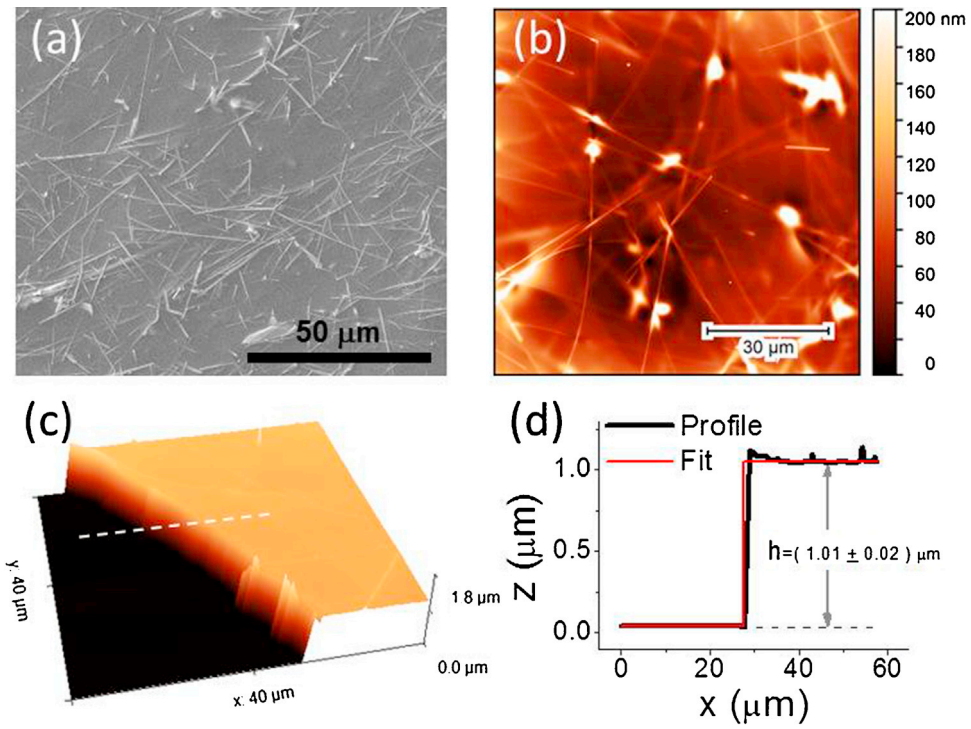

Fig. 3. Characterization of the AgNWs-PMMA nanocomposite film. A SEM image (a) shows the surface of the nanocomposite film after the thermal curing. AFM images showing the surface features of the film (b) and a step height (c) formed by scratching it to determine its thickness. A height profile across the line drawn in (c) is shown in (d). The film thickness was obtained from a fit of the step profile.

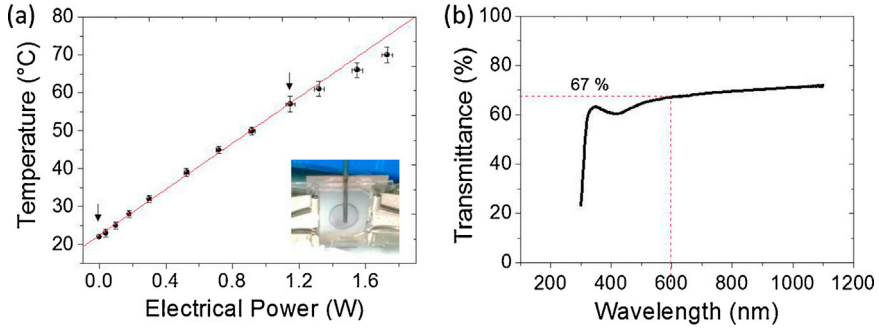

Fig. 4. Calibration of the electrothermal device (a) and optical transmittance of the AgNWs-PMMA nanocomposite film (b). Arrows in fig. (a) mark the interval of the linear regression calculation.

Although the absorption at 520 nm seems to increase as well, one should consider that the band centered at 664 nm is broad and a tale is superimposed to the first band. Pictures of the device before and during the heating showing the characteristic coloration of the solution are displayed in Fig. 5c and d respectively.

3.2. Phase transition of pNIPAM

In another set of experiments, the AgNWs-PMMA nanocomposite was applied successfully as an electrothermal ink on the external side walls of a test tube and cured at room temperature. A track of the nanocomposite ink was formed surrounding the bottom of the tube as indicated by the red lines in Fig. 6a and thin copper wires were contacted on both extremes with silver paste. A certain amount of the pNIPAM 2% wt. solution was poured in the tube. When the DC power was supplied, the increment in temperature above the LCST triggered the transition and the solution turned opaque. Below the LCST, the polymer is hydrophilic and therefore soluble in water, forming a clear transparent aqueous solution. However, above the LCST, the chain structure of the polymer becomes hydrophobic and collapses. The solution becomes turbid and the polymer precipitates. It is worth mentioning that the LCST is barely independent of the polymer concentration or the molecular weight, providing an excellent reproducible test system for our electrothermal device [20].

In addition, the phase transition of pNIPAM was observed by dispensing a carboxylic-terminated pNIPAM solution (0.5% wt.) into the reservoir of the device. The optical transmittance and the trends at 550 nm were followed by UV–vis by acquiring spectra each 5 s while temperature was externally controlled. The voltage was set at 3 V but cycled by switching the power supply ON and OFF with a programmed relay. The cycle time was 5 min. When the state was ON, the current measured was (0.15 ± 0.01) A, giving a total electrical power of (0.45 ± 0.03) W and a final temperature of 36 °C according to the calibration shown in Fig. 4. Photographs of the device at low and high temperatures are shown in Fig. 6b. The

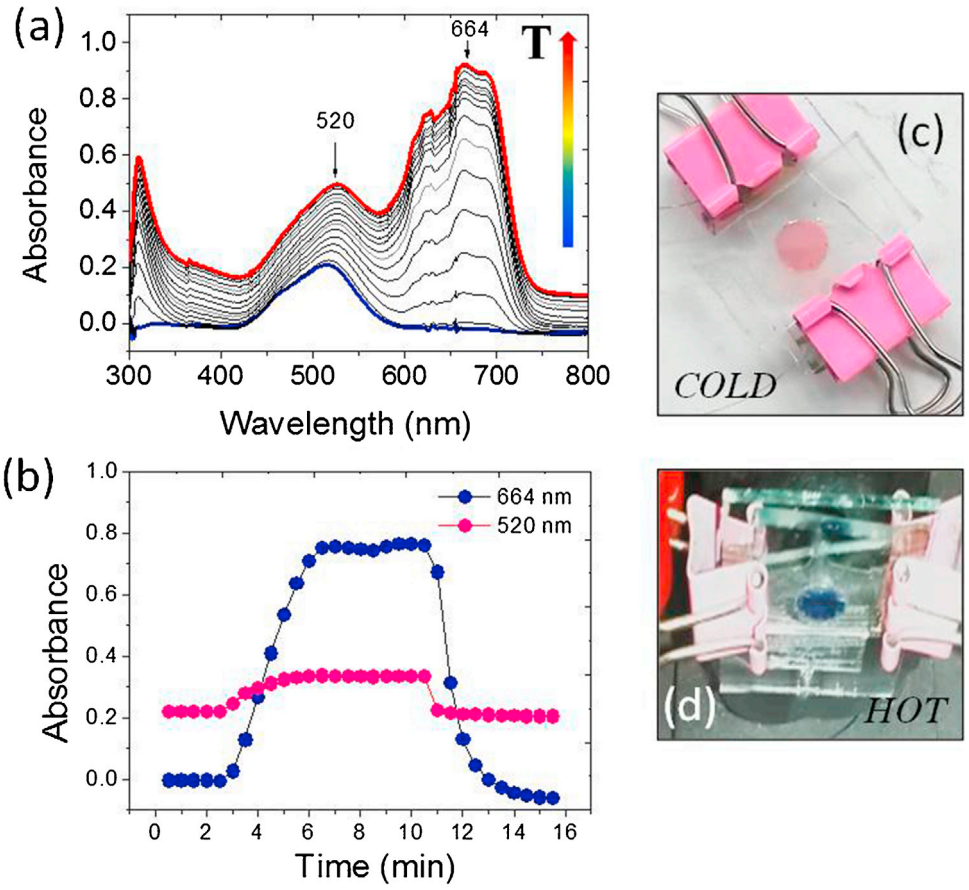

Fig. 5. Application of the electrothermal device in the thermal equilibrium of a $[Co(H_2O)_6]^{2+}/[CoCl_4]^{2-}$ aqueous solution. The evolution of the absorption spectrum from the cold (blue curve) to the hot (red curve) (a), the absorption maxima at 520 nm and 664 nm after the subtraction of the baseline (b) and optical images of the device in the cold (c) and hot (d) states. (For interpretation of the references to colour in this figure legend, the reader is referred to the web version of this article.)

evolution of the transmittance spectra during the heating cycle is shown in Fig. 6c. In Fig. 6d it can be seen that the electrothermal control provided by the AgNWs network is effective in cycling the temperature and triggering the solubility phase transition of pNIPAM. It is interesting noticing that the low and high transparency switches require low electrical power input, as the LCST is around 32 °C. However, for the first cycle, a delay of 27 s was observed after the power was switched ON and the transition from high to low transmittance begun. This should be the time required for the temperature to surpass the LCST. Another delay of 117 s was observed after turning the power OFF (first cooling cycle) and the system begun to return to a high transmittance value. As previously mentioned, the solution should reach approximately 36 °C during the ON state, *i.e.* 4 °C above the LCST. The required time to cool down explains the delay observed. In the following cycles, the time delays are reduced to 11–12 s for the heating branch and to 106–112 s for the cooling branch. The reversibility of the phase transition in pNIPAM was clearly observed; however, a small decay in the transmittance of the cycled profile was noticed. This may be caused by remaining aggregates of pNIPAM due to the absence of agitation in the reservoir, or because the final temperature during cooling might have not reached the starting value. This last argument also explains the reduction in the time-delays of the transition after the ON and OFF switching.

Further studies of the pNIPAM transition could be easily pursued using the electrothermal device; for example, by adding a co-solvent, *e.g.* methanol, the LCST can be reduced [28], together with the thermal capacity of the liquid, therefore reducing the thermal inertia of the system and producing a faster transition. Adding salts to the solution is also known to produce a reduction in the LCST [29]. We call the attention to the fact that the thermoresponsivity of pNIPAM has been extensively studied for a number of applications. Because the LCST is in the window of many biological processes, like cell culture and protein denaturation, thermoresonsive surfaces containing pNIPAM are commonly employed in biochemistry and biology. In fact, the inclusion of an electrothermal nanocomposite layer in thermoresponsive surfaces may provide an extra feature for biological studies [30]. Also, attention should be paid to the integration of AgNWs-PMMA electrothermal films in smart windows technologies using pNIPAM hydrogels and other thermoresponsive materials, as well as in lab-on-a-chip microfluidic systems [31].

3.3. Synthesis of gold nanoparticles

In a final experiment, we used the electrothermal device as a reactor where a precursor, a reducer and a stabilizing agent in solution are thermally triggered to start the nucleation and growth of AuNPs. In this case, a stock solution containing 5.45 mg of $AuCl_3{\cdot}3H_2O$ and 150 μl of oleylamine in 2 ml of benzyl ether was prepared. The reservoir of the device was filled with the stock solution and aligned to the optical path of a UV–vis spectrophotometer. The acquisition of the absorption spectra was programmed to occur at a 60 s cycle time. After the first two minutes, the power supply, set at a constant value of 5.5 V, was turned ON and a current of (0.15 ± 0.01) A was measured, corresponding to an electrical power of (0.82 ± 0.06) W. According to the calibration performed,

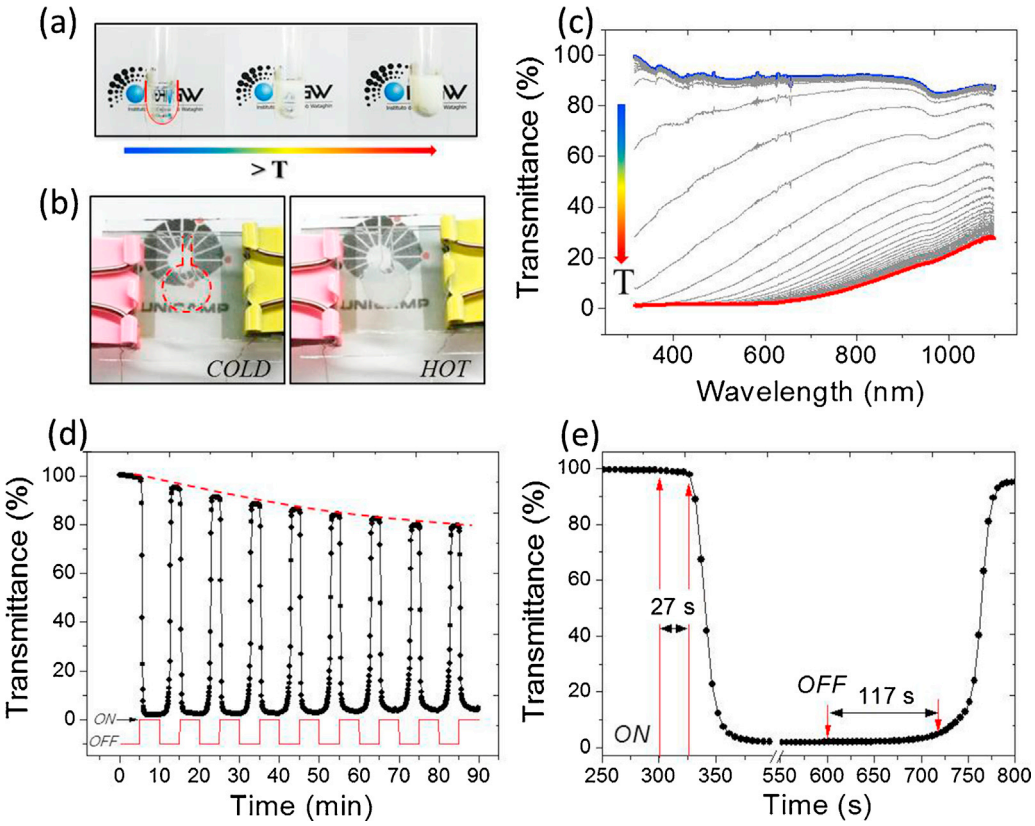

Fig. 6. In-situ characterization of the LSCT of carboxylic acid terminated pNIPAM aqueous solution. (a) Pictures of the transition observed on test tubes through the electrothermal control provided by AgNWs ink tracks deposited on the sides walls (marked with red lines). (b) The electrothermal device in the cold (left) and hot (right) states. (c) The evolution of the transmittance spectra during the transition. (d) The thermal cycling during the electrothermal switching ON-OFF using the electrothermal device. (e) Insights into the delay times of the transition when powering ON and OFF during the first cycle. (For interpretation of the references to colour in this figure legend, the reader is referred to the web version of this article.)

this value of electrical power corresponds to a final temperature of 48 °C.

We found that the formation of the LSPR could be easily registered and used for further analysis and modeling using Mie's scattering theory. Fig. 7a shows the evolution of the absorption spectra, in which an absorption band peaked at 537 nm develops, announcing the characteristics of the LSPR of AuNPs. The amplitude and broadness of the LSPR absorption band is related to the size and concentration of AuNPs in the colloid solution. On the other hand, at prolonged times, the band becomes asymmetrical and red-shifted, indicating plasmonic interactions among AuNPs. After 1 h of reaction, the power supply was turned OFF and the acquisition stopped. The content of the reservoir was extracted and dispersed in 1 ml of *n*-hexane inside an eppendorf tube. As can be seen in the inset of Fig. 7b, the inner walls of the device present a bluish-gray, explaining the broad blue-shifted spectrum due to deposition of AuNPs on the inner surfaces of the device. However, the extracted colloid shows a reddish/pink coloration characteristic of small size spherical AuNPs. Interestingly, nucleation of AuNPs was observed in the inner surface of the glass cover and not on the AgNWs-PMMA surface, showing that AgNWs are not exposed to the solutions and do not act as nucleating agents.

The extracted colloid was characterized in three different ways: firstly, the absorption spectra was acquired and submitted to further analysis (see below); secondly, dynamical light scattering (DLS) measurements were performed in order to estimate the mean size and size distribution of the AuNPs; finally, transmission electron microscopy (TEM) was performed to directly observe the AuNPs and remaining residues of the reaction. The absorption spectra of the extracted AuNPs was analyzed by performing a calculation based on Mie's scattering theory by considering small spherical nanoparticles for which the dipolar approximation applies [32]. Under this approximation, the total absorption of the colloid (Λ), assuming there are no plasmonic interactions between particles, is proportional to the absorption cross section and can be expressed as [33]

$$\Lambda = \frac{n_p C_{abs} h}{\ln(10)} = \frac{N_{NP} C_{abs}}{ln(10)} = \frac{N_{NP} k Im[\alpha]}{ln(10)} = \frac{24\pi^2 N_{NP} N^3 r^3}{ln(10)\lambda} \frac{Im[\varepsilon_{NP}]}{\left(\left(Re[\varepsilon_{NP}] + 2N^2\right)^2 + Im[\varepsilon_{NP}]^2\right)} \quad (2)$$

In this equation, n_p is the number of particles per unit volume and h is the thickness of the reservoir region, *i.e.* the PDMS spacer layer. The product of these two quantities gives the number of particles per unit area of the reservoir, N_{NP}. The wavevector $k = 2\pi/\lambda$ is multiplied by the imaginary part of the polarizability, α, to give the absorption cross section C_{abs}. The refractive index of the dielectric medium and the nanoparticle radius are N and r respectively.

For the calculation of the cross section, the dielectric function of the AuNPs (ε_{NP}) should be considered. This function can be calculated as a correction of the dielectric function of the bulk material. In this case, we use the bulk values of the dielectric function of gold as reported by Johnson and Christy [34], and the size dependent correction as expressed by Kreibig and Vollmer [35],

$$\varepsilon_{NP}(\omega, r) = \varepsilon_{bulk}(\omega) + \frac{\omega_p{}^2}{\omega^2 + i\omega\gamma_0} - \frac{\omega_p{}^2}{\omega^2 + i\omega\left(\gamma_0 + Av_f/r\right)} \quad (3)$$

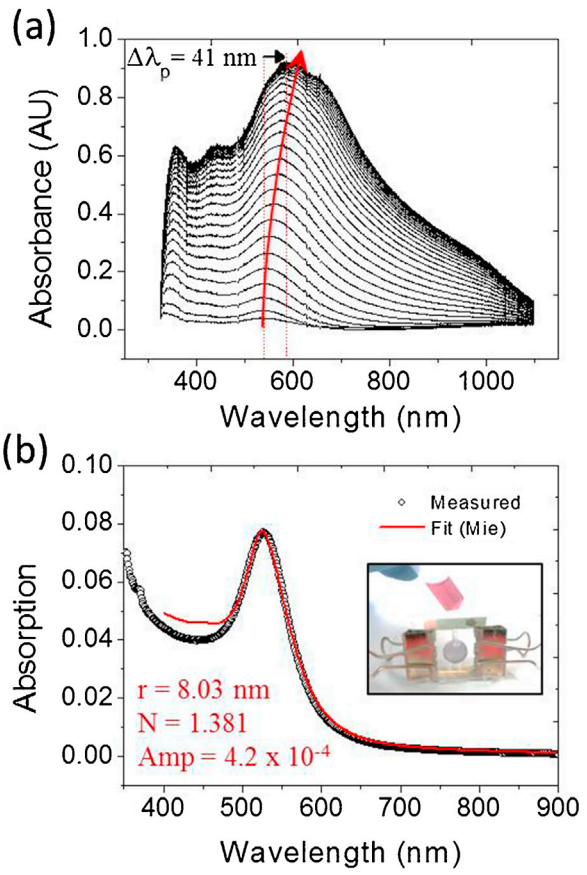

Fig. 7. Absorption spectra of AuNPs during the in-situ experiment (a) and after extraction and redispersion in *n*-hexane (b). The fitted absorption spectra as calculated using Mie's theory is superimposed with the measured spectra. Fitting parameters were: the amplitude constant multiplying the cross section (Amp), the nanoparticle radius (r) and the refractive index (N) of the dielectric surrounding medium.

where $\omega = c/\lambda$, ω_p is the plasma frequency, v_f is the Fermi velocity, and γ_0 is the damping frequency. The parameter A is a value close to unity that accounts for the interface between the nanoparticles and a dielectric supporting surface; in this case, for unsupported AuNPs we used $A = 1$ [36].

Fig. 7b shows the excellent agreement between the fitted absorption and the acquired spectra for the AuNPs in *n*-hexane. The fitting parameters were the particle radius, *r,* the refractive index of the dielectric medium, *N,* and the coefficient multiplying the cross section, *Abs = Np/ln(10).* The calculation results in a nanoparticle radius of 8 nm (16 nm in diameter), which is in good agreement with the diameter of the AuNPs as determined by DLS ($d = (18 \pm 2)$ nm, Fig. 8a) and TEM (Fig. 8b,c). Interestingly, a large population of small size of AuNPs with mean size (2.5 ± 0.5) nm is visualized by TEM that could not be detected by DLS nor the optical fitting of the absorption spectra. Most probably the synthesis resulted in a delayed or continuous nucleation due to the low temperature employed. The temperature dependence of the nucleation and growth mechanism could be one of the subjects to be studied by this method.

4. Conclusions

A nanocomposite ink containing AgNWs in a PMMA solution was successfully applied on glass slides to produce conductive films, 1 μm thick, with an optical transmittance of 67% and a sheet resistance of $(2.0 \pm 0.1)\ \Omega\,\mathrm{sq}^{-1}$. The films were used as an electrothermal element in a device that could be successfully used to observe in real time the optical transitions of three different physicochemical processes. For the case of cobalt chloride aqueous complex solutions we were able to follow the change in the absorption spectra of the bands centered at 520 nm (pink) and at 664 nm (blue) as the temperature increases. The experiment shows the change in the chemical equilibrium when the temperature is increased and the endothermic nature of the reaction that substitute the water molecules in the coordination sphere by Cl^- ions. By using the electrothermal device to follow the solubility transition of a pNIPAM aqueous solution, we were able to study the reversibility of the transition and the time delays associated with the heat dynamics in the small volume of the cavity, all by externally cycling the supplied power. Gold nanoparticles were synthetized in the reaction vessel of the device using $AgCl_3$ in the presence of oleylamine by triggering the nucleation using the electrothermal control. It was possible to follow in real time the evolution of the optical absorption due to the gold plasmon resonance. Further analysis of the obtained particles show a large population of AuNPs of small size ($d < 3$ nm) and spherical AuNPs of $d = (18 \pm 2)$ nm. TEM and DLS results are consistent with the Mie calculations of the absorption spectra.

We want to emphasize that the cases considered in this work are mere examples of the potential applications for the proposed device and for the nanocomposite ink. Moreover, electrothermal active thin films based on the AgNWs-PMMA nanocomposite could be integrated on lab-on-a-chip technologies for biochemical essays, smart windows and microelectronics.

5. Methods

$AgNO_3$ 99.9999%, ethylene glycol (EtGOH) anhydrous (99.8%), PVP 360000 mol wt., $FeCl_3$ and carboxylic acid terminated pNIPAM (average Mn 10000) were purchased from Sigma-Aldrich Co. and used without further purification. PMMA 7% wt. in chlorobenzene resist (PMMA C7) was purchased from MicroChem Corp, USA. PDMS Sylgard 184 was purchased from Dow Chemical Company, USA. Absorption/transmittance spectra were acquired in a Agilent Cary 8454 UV–vis spectrophotometer with the ChemStation Biochemical Add-On software installed (kinetics module). Electron microscopy and AFM were performed at LNNano, CNPEM, Campinas, Brazil. SEM images were acquired in a FEI Quanta 650 FEG microscope operated at 20 kV. TEM images were obtained with a JEM 2100 equipped with a LaB_6 filament and operated at 200 kV. AFM images were obtained using a Park NX10 in tapping mode at 287 kHz with a silicon tip Tap300-G from Budget Sensors. Images were processed using the free software Gwyddion 2.42.

Silver Nanowires were synthesized by slowly adding 0.2 g of PVP in 15 ml of EtGOH. In another flask, 0.25 g of $AgNO_3$ were dissolved in 10 ml of EtGOH and stirred for 1 h in darkness. After complete dissolution of both solutions they were mixed in a 200 ml round flask and 3.25 g of a 0.6 mM solution of $FeCl_3$ in EtGOH were rapidly added. The round flask was sealed and, without agitation, placed into an oven pre-heated at 130 °C, was kept for 5 h. AgNWs were extracted after synthesis by adding excess acetone and three steps of centrifugation and redispersion in isopropanol (IPA). AgNWs were finally dispersed in IPA in a concentration of $2.5\ \mathrm{g\,L}^{-1}$. For the preparation of the PDMS spacer, the two components of the Sylgard 184 kit were vigorously mixed in a 10:1 proportion and placed in a vacuum chamber for degasing. The homogenized mixture was then poured in a square flat mold filling approximately 2 ml height. The mold was then placed in an oven at 70 °C for 2 h. Cobalt chloride solution was prepared by adding concentrated HCl to a Co powder. After reaction, when a blue color solution was formed, 5 ml of the solution was filtered through a 0.22 μm pore PES filter and placed

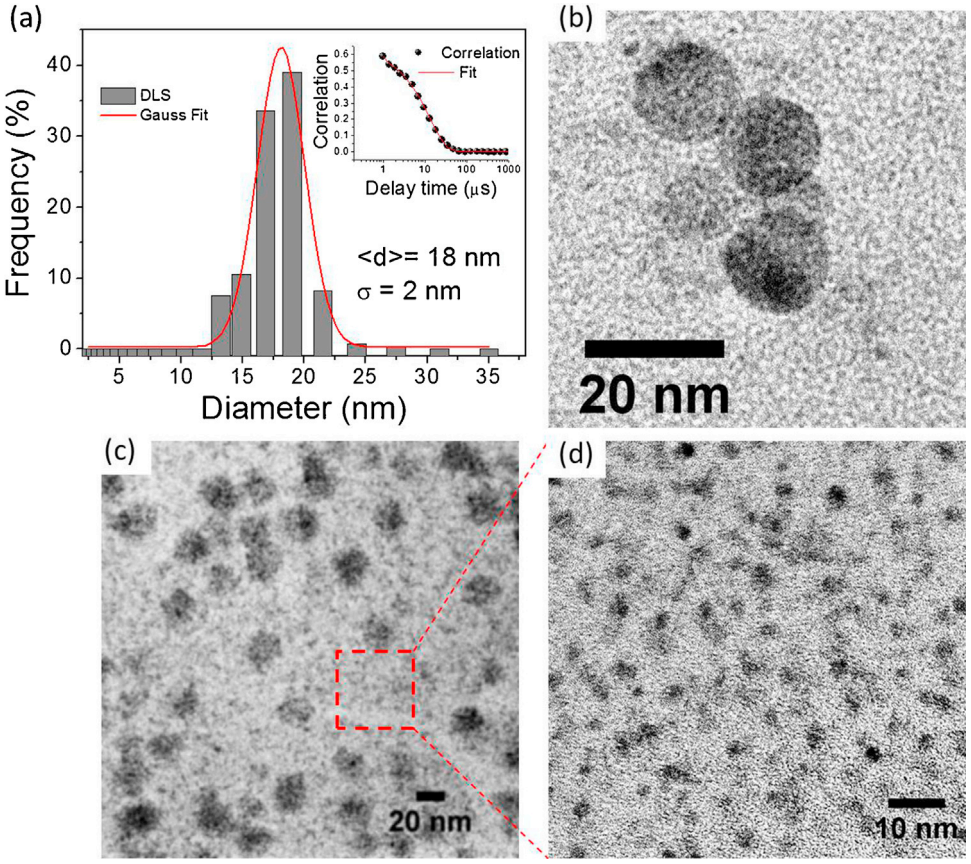

Fig. 8. (a) Particle size distribution and correlation function fitting (inset) as obtained by DLS. (b) TEM images showing the size and distribution of AuNPs extracted from the device after the in-situ experiment.

in a test tube. Deionized water (MilliQ, 18.4 MΩ) was slowly added until a color change was observed to form the final pink solution.

Acknowledgements

This work was supported and performed under the auspices of the Brazilian agencies CAPES, CNPq and FAPESP through Grants # 2011/19924-2, 2012/04870-7, 2012/05903-6, 2015/21290-2, and 2015/21289-4. EDM acknowledges the post-doctoral FAPESP fellowship # 2015/23882-4. The SEM, TEM and AFM data were acquired in the LNNano at the Centro Nacional de Pesquisa em Energia e Materiais (CNPEM) in Campinas-SP, Brazil. HP acknowledges support from ANPCyT-FONCyT PICT 2012-0770.

References

[1] D. Anh Dinh, K. Nam Hui, K. San Hui, J. Singh, P. Kumar, W. Zhou, Silver nanowires a promising transparent conducting electrode material for optoelectronic and electronic applications, Rev. Adv. Sci. Eng. 2 (2013) 324–345, http://dx.doi.org/10.1166/rase.2013.1048.
[2] A.R. Madaria, A. Kumar, F.N. Ishikawa, C. Zhou, Uniform, highly conductive, and patterned transparent films of a percolating silver nanowire network on rigid and flexible substrates using a dry transfer technique, Nano Res. 3 (2010) 564–573, http://dx.doi.org/10.1007/s12274-010-0017-5.
[3] T. Tokuno, M. Nogi, M. Karakawa, J. Jiu, T.T. Nge, Y. Aso, K. Suganuma, Fabrication of silver nanowire transparent electrodes at room temperature, Nano Res. 4 (2011) 1215–1222, http://dx.doi.org/10.1007/s12274-011-0172-3.
[4] N.M. Abbasi, H. Yu, L. Wang, Zain-ul-Abdin, W.A. Amer, M. Akram, H. Khalid, Y. Chen, M. Saleem, R. Sun, J. Shan, Preparation of silver nanowires and their application in conducting polymer nanocomposites, Mater. Chem. Phys. 166 (2015) 1–15, http://dx.doi.org/10.1016/j.matchemphys.2015.08.056.
[5] M.S. Miller, J.C. O'Kane, A. Niec, R.S. Carmichael, T.B. Carmichael, Silver nanowire/optical adhesive coatings as transparent electrodes for flexible electronics, ACS Appl. Mater. Interfaces 5 (2013) 10165–10172, http://dx.doi.org/10.1021/am402847y.
[6] H. Moon, P. Won, J. Lee, S.H. Ko, Low-haze, annealing-free, very long Ag nanowire synthesis and its application in a flexible transparent touch panel, Nanotechnology 27 (2016) 295201, http://dx.doi.org/10.1088/0957-4484/27/29/295201.
[7] L. Hu, H.S. Kim, J. Lee, P. Peumans, Y. Cui, Scalable coating and properties of transparent, flexible, silver nanowire electrodes, ACS Nano 4 (2010) 2955–2963, http://dx.doi.org/10.1021/nn1005232.
[8] A.R. Madaria, A. Kumar, C. Zhou, Large scale, highly conductive and patterned transparent films of silver nanowires on arbitrary substrates and their application in touch screens, Nanotechnology 22 (2011) 245201, http://dx.doi.org/10.1088/0957-4484/22/24/245201.
[9] E.D. Martínez, J.H. Lohr, M. Sirena, R.D. Sánchez, H. Pastoriza, Silver nanowires in poly (methyl methacrylate) as a conductive nanocomposite for microfabrication, Flex. Print. Electron. 1 (2016) 1–10, http://dx.doi.org/10.1088/2058-8585/1/3/035003.
[10] J.-G. Lee, J.-H. Lee, S. An, D.-Y. Kim, T.-G. Kim, S.S. Al-Deyab, A.L. Yarin, S.S. Yoon, Highly flexible, stretchable, wearable, patternable and transparent heaters on complex 3D surfaces formed from supersonically sprayed silver nanowires, J. Mater. Chem. A 5 (2017) 6677–6685, http://dx.doi.org/10.1039/C6TA10997G.
[11] T. Kim, Y.W. Kim, H.S. Lee, H. Kim, W.S. Yang, K.S. Suh, Uniformly interconnected silver-Nanowire networks for transparent film heaters, Adv. Funct. Mater. 23 (2013) 1250–1255, http://dx.doi.org/10.1002/adfm.201202013.
[12] S. Kiruthika, R. Gupta, G.U. Kulkarni, Large area defrosting windows based on electrothermal heating of highly conducting and transmitting Ag wire mesh, RSC Adv. 4 (2014) 49745–49751, http://dx.doi.org/10.1039/C4RA06811D.
[13] X. He, A. Liu, X. Hu, M. Song, F. Duan, Q. Lan, J. Xiao, J. Liu, M. Zhang, Y. Chen, Q. Zeng, Temperature-controlled transparent- film heater based on silver nanowire –PMMA composite film, Nanotechnology 27 (2016).
[14] J. Yeo, G. Kim, S. Hong, J. Lee, J. Kwon, H. Lee, H. Park, W. Manoroktul, M.-T. Lee, B.J. Lee, C.P. Grigoropoulos, S.H. Ko, Single nanowire resistive nano-heater for highly localized thermo-Chemical reactions: localized hierarchical heterojunction nanowire growth, Small (2014) 1–8, http://dx.doi.org/10.1002/smll.201401427.
[15] H. Lee, J. Yeo, J. Lee, H. Cho, J. Kwon, S. Han, S. Kim, S. Hong, S.H. Ko, Selective thermochemical growth of hierarchical ZnO nanowire branches on silver

nanowire backbone percolation network heaters, J. Phys. Chem. C 121 (2017) 22542–22549, http://dx.doi.org/10.1021/acs.jpcc.7b08129.
[16] P. Zhang, I. Wyman, J. Hu, S. Lin, Z. Zhong, Y. Tu, Z. Huang, Y. Wei, Silver nanowires: synthesis technologies, growth mechanism and multifunctional applications, Mater. Sci. Eng. B Solid-State Mater. Adv. Technol. 223 (2017) 1–23, http://dx.doi.org/10.1016/j.mseb.2017.05.002.
[17] F. Basarir, F.S. Irani, A. Kosemen, B.T. Camic, F. Oytun, B. Tunaboylu, H.J. Shin, K.Y. Nam, H. Choi, Recent progresses on solution-processed silver nanowire based transparent conducting electrodes for organic solar cells, Mater. Today Chem. 3 (2017) 60–72, http://dx.doi.org/10.1016/j.mtchem.2017.02.001.
[18] Q. Zhao, M. Zhao, J. Qiu, W.Y. Lai, H. Pang, W. Huang, One dimensional silver-based nanomaterials: preparations and electrochemical applications, Small 13 (2017) 1–18, http://dx.doi.org/10.1002/smll.201701091.
[19] M.A. Haq, Y. Su, D. Wang, Mechanical properties of PNIPAM based hydrogels: a review, Mater. Sci. Eng. C 70 (2017) 842–855, http://dx.doi.org/10.1016/j.msec.2016.09.081.
[20] A. Halperin, M. Kröger, F.M. Winnik, Poly(N-isopropylacrylamide) phase diagrams: fifty years of research, Angew. Chem. Int. Ed. 54 (2015) 15342–15367, http://dx.doi.org/10.1002/anie.201506663.
[21] J. Turkevich, P.C. Stevenson, J. Hillier, A study of the nucleation and growth processes in the synthesis of colloidal gold, Discuss. Faraday Soc. 11 (1951) 55–75, http://dx.doi.org/10.1039/DF9511100055.
[22] M. Brust, M. Walker, D. Bethell, D.J. Schiffrin, R. Whyman, Synthesis of thiol-derivatised gold nanoparticles in a two-phase Liquid–Liquid system, J. Chem. Soc. Chem. Commun. 0 (1994) 801–802, http://dx.doi.org/10.1039/C39940000801.
[23] S. Mourdikoudis, L.M. Liz-Marzán, Oleylamine in nanoparticle synthesis, Chem. Mater. 25 (2013) 1465–1476, http://dx.doi.org/10.1021/cm4000476.
[24] X. Liu, M. Atwater, J. Wang, Q. Dai, J. Zou, J.P. Brennan, Q. Huo, A study on gold nanoparticle synthesis using oleylamine as both reducing agent and protecting ligand, J. Nanosci. Nanotechnol. 7 (2007) 3126–3133, http://dx.doi.org/10.1166/jnn.2007.805.
[25] Y. Sun, Y. Xia, Large-Scale synthesis of uniform silver nanowires through a soft, self-Seeding, polyol process, Adv. Mater. 14 (2002) 833, http://dx.doi.org/10.1002/1521-4095(20020605)14:11<833:AID-ADMA833>3.0. CO;2-K.
[26] J. Jiu, T. Araki, J. Wang, M. Nogi, T. Sugahara, S. Nagao, H. Koga, K. Suganuma, E. Nakazawa, M. Hara, H. Uchida, K. Shinozaki, Facile synthesis of very-Long silver nanowires for transparent electrodes, J. Mater. Chem. A 2 (2014) 6326, http://dx.doi.org/10.1039/c4ta00502c.
[27] J. Wang, J. Jiu, T. Araki, M. Nogi, T. Sugahara, S. Nagao, H. Koga, P. He, K. Suganuma, Silver nanowire electrodes: conductivity improvement without post-treatment and application in capacitive pressure sensors, Nano-Micro Lett. 7 (2014) 51–58, http://dx.doi.org/10.1007/s40820-014-0018-0.
[28] M.F. Winnik, S.H. Ottaviani, M. Bossmann, N.J. Garcia-Garibay, Cononsolvency of poly(N-isopropylacrylamide) in mixed water-methanol solutions: a look at spin-labeled polymers, Macromolecules 25 (1992) 6007–6017, 0024-9297/92/2226-6.
[29] Y.J. Zhang, S. Furyk, D.E. Bergbreiter, P.S. Cremer, Specific Ion effectis on the water solubility of acromolecules: PNIPAM and the Hofmeister series, J. Am. Chem. Soc. 127 (2005) 14505–14510, http://dx.doi.org/10.1021/Ja0546424.
[30] Y. Guan, Y. Zhang, PNIPAM microgels for biomedical applications: from dispersed particles to 3D assemblies, Soft Matter. 7 (2011) 6375, http://dx.doi.org/10.1039/c0sm01541e.
[31] N.Y. Lee, Recent progress in lab-on-a-Chip technology and its potential application to clinical diagnoses, Int. Neurourol. 17 (2013) 2–10.
[32] S.A. Maier, Plasmonics: Fundamentals and Applications, 1st ed., Springer Science+Business Media LLC, New York, 2007.
[33] E.D. Sánchez, M.L. Martínez, H. Martínez Ricci, G.J.A.A. Troiani, Optical properties of Au nanoparticles included in mesoporous TiO_2 thin films: a dual experimental and modeling study, J. Phys. Chem. C 117 (2013) 7246–7259, http://dx.doi.org/10.1021/jp3127847.
[34] P.B. Johnson, R.W. Christy, Optical constants of the noble metals, Phys. Rev. B. 6 (1972) 4370–4379, http://dx.doi.org/10.1103/PhysRevB.6.4370.
[35] U. Kreibig, M. Vollmer, Optical Properties of Metal Clusters, 1st ed., Springer-Verlag Berlin, Heidelberg: Berlin, 1995.
[36] V. Amendola, M. Meneghetti, Size evaluation of gold nanoparticles by UV–vis spectroscopy, J. Phys. Chem. C 113 (2009) 4277–4285, http://dx.doi.org/10.1021/jp8082425.

Biography

Eduardo D. Martínez is an assistant researcher of CONICET at the Bariloche Atomic Center (CAB), San Carlos de Bariloche, Río Negro, Argentina. At the moment, he is working in the Physics Department at the Universidad Estadual de Campinas (UNICAMP), Brazil, with a postdoctoral fellowship from FAPESP. He obtained a degree in materials engineering in 2008 at the Instituto J. A. Sabato, University of San Martín (UNSAM), Argentina. He obtained his PhD in 2013 at UNSAM. His PhD thesis, on the subject of mesoporous thin films loaded with plasmonic nanoparticles, was awarded by the Insitute J. A. Sabato as Best PhD Thesis in the field of Science and Technology of Materials for the period 2012–2014. He performed a postdoctoral research at CAB-Argentina developing nanocomposite materials for microfabrication. His expertise is in the field of chemistry of nanomaterials and nanocomposites, mostly applied to plasmonics, photonics and microfabrication.